

Dynamic behavior and driving region of spray combustion instability in a backward-facing step combustor

Kenta Kato,¹ Hiroyuki Hashiba,¹ Jun Nagao,² Hiroshi Gotoda ,^{1,*} Yusuke Nabae,¹ and Ryoichi Kurose ²

¹*Department of Mechanical Engineering, Tokyo University of Science, 6-3-1 Nijjuku, Katsushika-ku, Tokyo 125-8585, Japan*

²*Department of Mechanical Engineering and Science, Kyoto University, Kyoto daigaku-Katsura, Nishikyo-ku, Kyoto 615-8540, Japan*



(Received 16 February 2024; accepted 20 June 2024; published 6 August 2024)

We numerically study the dynamic behavior and driving region of spray combustion instability in a backward-facing step combustor using analytical methodologies based on dynamical systems theory, symbolic dynamics, complex networks, and machine learning. The global dynamic behavior of a heat release rate field represents low-dimensional chaotic oscillations with deterministically aperiodic intercycle dynamics. Spray combustion instability is driven in the formation and separation region of a large-scale organized vortex induced by the hydrodynamic shear layer instability at the edge of the backstep. This region corresponds fairly to that of the hub in an acoustic-energy-flux-based spatial network. The feature importance in a random forest is valid for clarifying the feedback coupling of spray combustion instability.

DOI: [10.1103/PhysRevE.110.024204](https://doi.org/10.1103/PhysRevE.110.024204)

I. INTRODUCTION

Combustion instability is a self-excited nonlinear phenomenon stemming from the amplification of natural acoustic resonance modes in a confined combustion system due to a mutual interplay among pressure, heat release rate, and flow velocity fields [1]. The incidence and subsequent sustainment of combustion instability can lead to the profound structural breakage of various combustors involving ground-based gas turbines and aircraft engines through strong mechanical vibrations of the combustor and the local increase in the quantity of heat transfer to the combustor wall. The flow field in these combustors basically consists of shear flow. The roll up of a shear layer and the breakdown of vortices affect a feedback loop of acoustic pressure and heat release rate fluctuations during combustion instability. A backward-facing step combustor is one of the simplest configurations for examining the dynamics of combustion instability. A well-recognized physical mechanism of combustion instability in this type of combustor is that the large-scale organized vortex from the backstep induces large changes in heat release rate fluctuations, thereby forming a strong feedback loop. This has been intensively investigated in many experimental and numerical studies [2–7].

One of the most typical complex chemically reacting two-phase turbulent flows is spray combustion accompanied by elementary processes via fuel atomization, droplet dispersion, and droplet evaporation. Spray combustion potentially allows the emergence of a rich variety of spatiotemporal dynamic behaviors in thermoacoustic systems. Kurose and co-workers [8–10] have recently conducted three important numerical studies on spray combustion instability in a backward-facing step combustor. They have shown the

importance of large-scale vortical motion near the dump plane due to the periodic oscillations of the inlet flow velocity in the driving of combustion instability. They have also clarified the effects of droplet size and temporal fluctuations in liquid fuel flow rate on the intensity of spray combustion instability.

Complex-systems-based analysis has recently yielded a new paradigm in the study of combustion instability and enabled us to provide an in-depth physical understanding and interpretation of nonlinear dynamics of combustion instability in various turbulent combustors such as swirl-stabilized combustors [11–28] and bluff-body-stabilized combustors [14–16,19,29–33]. The importance of complex-systems-based analysis has been emphasized by Sujith and co-workers [34,35]. In relation to combustion instability in a backward-facing step combustor, the randomness of acoustic pressure fluctuations has been examined by quantifying the permutation entropy based on symbolic dynamics [36]. Machine learning technologies derived from statistical learning theory have made remarkable advances in data-driven science and related fields of nonlinear physics. A wide variety of supervised machine learning technologies have recently stood out in terms of the aims to (i) create futuristic detectors of a portent of combustion instability and (ii) deeply comprehend the nonlinear dynamics of combustion instability [37–42]. The former aim has been attempted using a support vector machine [43] and a convolutional neural network [44], whereas the latter has been attempted by a reservoir computing [45] that belongs to a subclass of recurrent neural networks. However, many previous studies [21,22,36–42,46–48] were limited to gaseous combustion and did not explore the nonlinear dynamics and driving region of spray combustion instability in a backward-facing step combustor from the perspectives of complex-systems-based analysis and machine learning.

The purpose of this study is to clarify the nonlinear dynamics and driving region of spray combustion instability in a

*Contact author: gotoda@rs.tus.ac.jp

backward-facing step combustor by using analytical methods based on dynamical systems theory, symbolic dynamics, synchronization, complex networks, and machine learning. We mainly undertake an intensive analysis of acoustic pressure and heat release rate fluctuations, focusing on the following three points. First, we characterize the global dynamic behavior of spray combustion instability using the ordinal partition transition network (OPTN) entropy [49] in combination with surrogate data methods [50,51]. Second, we clarify the motion of an acoustic power source using an acoustic-energy-flux-based spatial network [48] and deduce the driving region of spray combustion instability using a symbolic dynamics-based synchronization index (SDSI) [42]. Finally, we clarify the directional coupling during spray combustion instability by a causality analysis based on a random forest [52]. Note that, similarly to Mori *et al.* [42], we exploit a random forest because it is applicable to the elucidation of the formation mechanism of spray combustion instability rather than the detection of a portent of spray combustion instability.

The remainder of this paper is organized as follows. A brief description of the numerical computation and analytical methods is provided in Sec. II. We present and discuss results in Sec. III. We summarize in Sec. IV.

II. NUMERICAL COMPUTATION AND ANALYTICAL METHODS

A. Numerical computation

In this study we apply complex-systems-based analysis and machine learning to the simulation data of the spatiotemporal structures obtained by a large-eddy simulation (LES) of spray combustion instability in a backward-facing step combustor [8–10]. The governing equations and boundary conditions are almost the same as those in previous studies [8–10]. Figure 1(a) shows the computational domain and conditions. Air is released from the inlet of the combustor, and fuel droplets are injected vertically upward from a position 5 mm upstream from the edge of a step, i.e., $x = -5$ mm. The temperature T and cross-sectional plane velocity U of the incoming air are set to 760 K and 50 m/s, respectively. The temperature $T_{L,inj}$ and velocity $V_{L,inj}$ of the incoming fuel droplets are set to 300 K and 2 m/s, respectively. We use a nonequilibrium Langmuir-Knudsen model [53–55] for the evaporation of fuel droplets. We employ the atomization model proposed by Lee *et al.* [56]. In this atomization model, the droplet-size distribution dynamically changes during fuel droplet injection by considering the cross-sectional plane average air velocity. The equivalence ratio is set to 1.2. Kitano *et al.* [8] have reported that both the dominant frequency and intensity of the acoustic pressure fluctuations remain almost unchanged even under a coarser-grained LES than the present study. We conduct a LES with a finer grid resolution than those reported in Refs. [8–10]. Note that the time resolution of the numerical computation is 0.001 ms. Figures 1(b) and 1(c) show time variations in spatially averaged pressure $\langle p \rangle$ and total heat release rate $\langle q \rangle$ inside the combustor. Both $\langle p \rangle$ and $\langle q \rangle$ exhibit a dominant frequency of approximately 700 Hz, which corresponds to the longitudinal acoustic mode in the combustor [9]. In this study we analyze the spatiotemporal data during well-developed

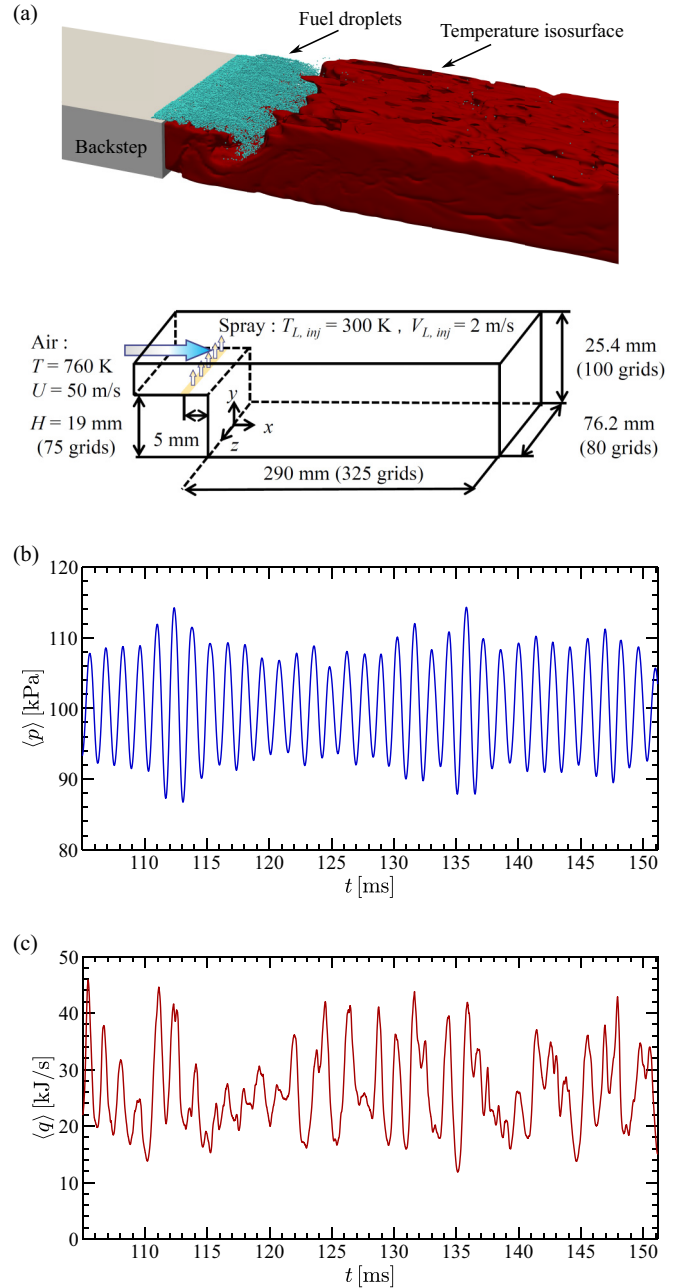


FIG. 1. (a) Computational domain and conditions. Time variations in (b) spatially averaged pressure $\langle p \rangle$ and (c) heat release rate $\langle q \rangle$ during spray combustion instability.

spray combustion instability at $t \geq 105$ ms after sufficiently removing the transient in numerical computation due to the injection initiation of the fuel droplets at $t = 75$ ms and the subsequent forced ignition.

B. The OPTN and surrogate data method

The OPTN [49,57] is a directed and weighted network constructed from the transition of permutation patterns in a time series. The importance of the OPTN to the analysis of combustion instability has been highlighted in many recent studies [25,42,58]. For the construction of the OPTN, we first

extract permutation patterns (rank-order patterns) $\Pi_{(q)}^{d_e}$ ($i = 1, 2, \dots, d_e!$) from $\{\langle q \rangle(t_i)\}_{i=1}^N$. Here d_e is the rank-order pattern length and N is the total number of data points. We define a node in the OPTN as Π . The transition probability w_{ij} from Π_i to Π_j is used as a link in the network. We estimate the OPTN entropy S_t defined as

$$S_t = \frac{-\sum_{i,j=1}^{d_e!} w_{ij} \log w_{ij}}{4 \log d_e!}. \quad (1)$$

Kulp and Zunino [59] reported the appearance of forbidden permutation patterns in a short time series of a stochastic process at $d_e \geq 6$. This means that a suitable value of d_e should be set at $d_e \leq 5$. In our preliminary test, we have examined the number of forbidden permutation transition patterns in the OPTN constructed from the stochastically fluctuating time series data of Brownian motion and white Gaussian noise, where the possible permutation transition patterns are $(d_e!)^2$. The forbidden permutation transition patterns in the OPTN appear at $d_e \geq 4$ for their data with 10000 data points. We set $d_e = 3$ for the estimation of S_t to prevent the onset of forbidden permutation transition patterns.

Schreiber and Schmitz [50] proposed an iterative amplitude-adjusted Fourier transform (IAAFT) surrogate method as one of the statistical tests to verify the presence of nonlinearity underlying a time series. This method enables us to obtain the time series data with almost the same probability distribution and power spectrum as the original data. The null hypothesis of the IAAFT surrogate method is that irregular components in the original data are generated by a linear stochastic process. Small *et al.* [51] proposed a pseudoperiodic (PP) surrogate method to verify the presence of deterministically nonperiodic intercycle dynamics in a time series. The null hypothesis of the PP surrogate method is that there is no determinism other than the periodic behavior in a time series. The null hypothesis can be rejected if there is a significant difference between the OPTN entropy values for the original and surrogate data. We prepare 1000 sets of the IAAFT and PP surrogate data in this study. To discern the significant difference between the values of S_t for the original and surrogate data, we set $N = 4618$ and $\Delta t = 0.01$ ms, corresponding to approximately 20 cycles of well-developed high-frequency combustion instability, where Δt is the time resolution of the analyzed $\langle q \rangle$.

C. The SDSI

Asami *et al.* [25] have proposed the SDSI for deducing the driving region of combustion instability. For the estimation of the SDSI, we first construct symbolic recurrence plots (SRPs) with the matrix element of $S_{R,ij}$ by color coding the time series of the acoustic pressure p' and heat release rate q' into $d_e!$ permutation patterns,

$$S_{R,ij} = \begin{cases} 1 & \text{for } \pi_{p'}^{d_e}(t_i) = \pi_{q'}^{d_e}(t_j) \\ 0 & \text{otherwise,} \end{cases} \quad (2)$$

where $\pi_{p'}^{d_e}(t_i)$ and $\pi_{q'}^{d_e}(t_j)$ denote the permutation patterns of p' and q' , respectively.

Here, S_{SI} is defined as the product of the determinism D_{sr} in SRPs and the synchronization parameter $r_{p'q'}$,

$$S_{SI} = D_{sr} r_{p'q'}, \quad (3)$$

$$D_{sr} = \frac{\sum_{l=l_{\min}}^{N_e-|\tau_a|} l P_l}{\sum_{l=1}^{N_e-|\tau_a|} l P_l}, \quad (4)$$

$$r_{p'q'} = \frac{1}{N} \left| \sum_{k=1}^N e^{i[\theta_{p'}(t_k) - \theta_{q'}(t_k)]} \right|, \quad (5)$$

where τ_a is the time distance between the main diagonal of $S_{R,ij}$ and the diagonal parallel to the main diagonal, l_{\min} is the minimum diagonal length, N is the number of data points in p' and q' , P_l represents the frequency distribution of the length l of each diagonal parallel to the main diagonal, and $N_e = N - d_e + 1$. Note that $\theta_{p'}$ and $\theta_{q'}$ denote the instantaneous phases of p' and q' , respectively, obtained by the Hilbert transform. The S_{SI} reflects not only the phase synchronization but also the recurrence between acoustic pressure and heat release rate fluctuations. It ranges from zero to unity and takes a high value as the mutual coupling between acoustic pressure and heat release rate fluctuations strengthens. In this study, we set $l_{\min} = 5$ and $N = 46177$. We set $d_e = 5$ for the estimation of D_{sr} in SRPs to prevent the onset of forbidden permutation patterns.

D. Acoustic-energy-flux-based spatial network

Krishnan *et al.* [33] proposed an undirected weighted network, i.e., a thermoacoustic power network, to deduce the acoustic power source during combustion instability in a bluff-body-stabilized turbulent combustor. They consider grid points in an OH* chemiluminescence intensity image as nodes of the network. These nodes are connected via a link when the product of acoustic pressure and heat release rate fluctuations at a node is positive. Kawano *et al.* [48] have proposed an acoustic-energy-flux-based spatial network as a new thermoacoustic power network for clarifying the motion of the acoustic power source in a subscale rocket engine combustor. In this network, the weight of the link between nodes is defined as the average of energy fluxes at the nodes. The energy outflow or induction is defined as the acoustic energy produced per unit volume and unit time. The acoustic energy flux I_{ij} that reaches another position \mathbf{x}_j via the generated acoustic energy at position \mathbf{x}_i is defined as

$$I_{ij} = \frac{|\Phi(\mathbf{x}_i) \Delta x \Delta y|}{2\pi |\mathbf{x}_i - \mathbf{x}_j|}, \quad (6)$$

where $\Phi(\mathbf{x}_i)$ is the acoustic energy produced at position \mathbf{x}_i , and Δx and Δy are each the length of each edge of the grid. In this study, unlike the method proposed in Ref. [48], we do not consider the acoustic energy source due to molecular production [60]. Let us assume that the acoustic power source $\Phi(\mathbf{x}_i)$ produced at position \mathbf{x}_i is calculated as $\Phi(\mathbf{x}_i) = \frac{p'_1(\mathbf{x}_i) q'_1(\mathbf{x}_i)}{p'_0(\mathbf{x}_i)}$. Here subscript 1 (0) is the fluctuation value (time-averaged value). We consider each grid in the computational domain as a node. The weight w_{ij} of the link between nodes is the average of the energy fluxes I_{ij} from the i th to j th nodes and

I_{ji} from the j th to i th nodes:

$$w_{ij} = \frac{1}{2}(I_{ij} + I_{ji}). \quad (7)$$

Similarly to the thermoacoustic power network proposed by Krishnan *et al.* [33], we connect links only between nodes with $\Phi(\mathbf{x}_i) > 0$ that amplify the acoustic power source. Thus, the weighted adjacency matrix A_{ij} is expressed as

$$A_{ij} = \begin{cases} w_{ij} & \text{for } i, j \neq 0, \Phi(\mathbf{x}_i) > 0, \Phi(\mathbf{x}_j) > 0 \\ 0 & \text{otherwise.} \end{cases} \quad (8)$$

The node strength s_i of the weighted network is defined as

$$s_i = \sum_{j=1}^M A_{ij}, \quad (9)$$

where M is the total number of nodes. Here, $M = 15\,325$ in this study, which corresponds to the analytical region ($-1 \leq x/H \leq 7$ and $0 \leq y/H \leq 1.3$ except for the surface of the backward-facing step). As shown in Eq. (9), s_i at a node is the summation of the link weight representing the transport degree of energy flux between a node i and other nodes j . A node with high s_i corresponds to a network hub representing the acoustic power source. An important point is that high node strength indicates the formation of an acoustic power source.

E. Random forest

A random forest [61] is a supervised machine learning for regression and classification using multiple decision trees. It is an ensemble learning method that enables the multiple random sampling of the training data to avoid over learning and the loss of learning accuracy. We can obtain highly accurate results for the entire decision tree by majority voting to classify problems and averaging for regression problems. Leng *et al.* [52] reported that the feature importance in a random forest can be used to estimate causality among features. In this study, we evaluate the spatial interaction between thermoacoustic and vorticity fields using the feature importance of a random forest. We define the feature importance as the sum of the mean-square error reduced by the split of each decision tree. Assuming that there is a total of T splits of each decision tree, the feature importance of m'_i on the target variable q' can be defined as

$$f_{m'_i \rightarrow q'} = \sum_{s=1}^T (E_{T^s} - E_{T^s}^1 - E_{T^s}^2) \Theta(T^s = i), \quad (10)$$

where E_{T^s} is the mean-square error from the T^s th split, $E_{T^s}^1$ and $E_{T^s}^2$ are the mean-square error from further splits, and $\Theta(T^s = i)$ is the indicator function. In addition, $\Theta = 1$ when the T^s th division is attributable to m'_i ; otherwise $\Theta = 0$. In this study, the total number of splits is set to $T = 100$.

III. RESULTS AND DISCUSSION

Figure 2 shows the frequency distribution of the OPTN entropy S_t for the surrogate and original data of the total heat release rate $\langle q \rangle$ inside the combustor. Note that we estimate S_t of $\langle q \rangle$ at $-1 \leq x/H \leq 7$. The values of S_t for both the

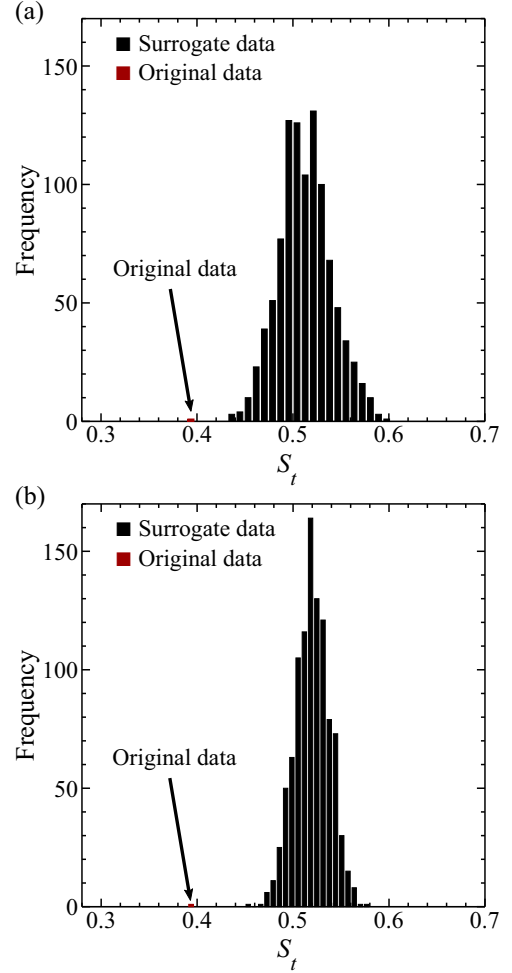


FIG. 2. Frequency distribution of the OPTN entropy S_t for the surrogate and original data of $\langle q \rangle$ during spray combustion instability: (a) IAAFT surrogate data and (b) PP surrogate data.

IAAFT and PP surrogate data do not coincide with those of the original data. The significant rejection of the null hypotheses indicates the presence of deterministically nonperiodic intercycle dynamics in a heat release rate field. The Rössler system with three degrees of freedom is a well-recognized low-dimensional nonlinear dynamical system and can create a low-dimensional deterministic chaos [62]. Godavarthi *et al.* [63] have recently studied the relevance of the Rössler system to a transition from combustion noise to combustion instability in a bluff-body-stabilized turbulent combustor. As shown in Fig. 1(c), the time variation in $\langle q \rangle$ is similar to that of the Rössler chaos. Small *et al.* [51] clearly showed that the Rössler chaos exhibits deterministically nonperiodic intercycle dynamics by estimating the correlation dimension in combination with the PP surrogate method. In our preliminary test, S_t takes approximately 0.35 for the Rössler chaos. This value roughly corresponds to that of the original $\langle q \rangle$. On the basis of the above findings, the global dynamic behavior of the heat release rate field represents low-dimensional chaotic oscillations. In this study, we have estimated S_t for a down-sampled time series of $\langle q \rangle$ with $N = 4618$ and $\Delta t = 0.01$ ms, but the null hypotheses of the surrogate data can be rejected

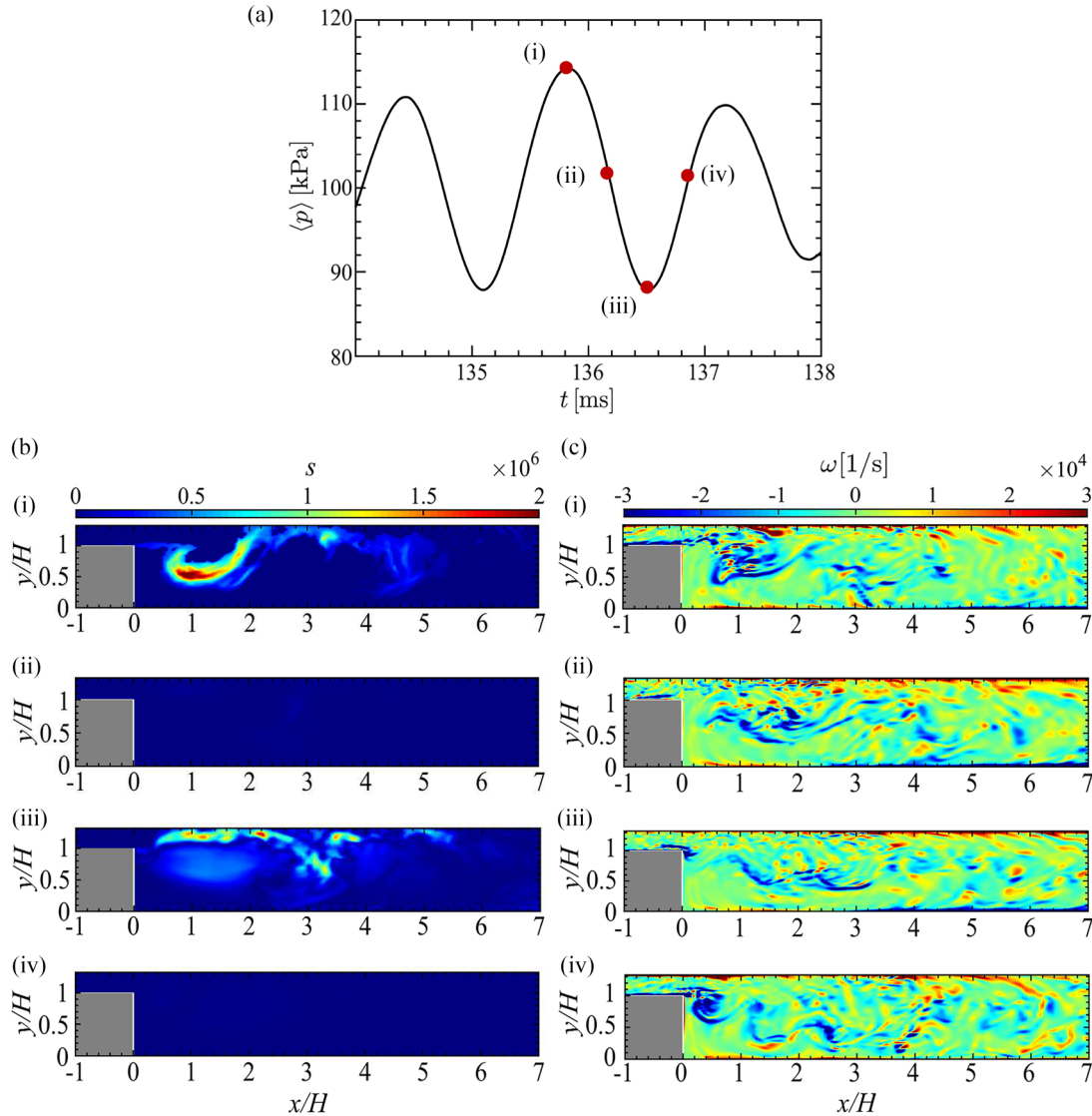


FIG. 3. (a) Time variation in the spatially averaged pressure field $\langle p \rangle$, (b) spatial distribution of node strength s in the acoustic-energy-flux-based spatial network, and (c) spatial distribution of vorticity ω during spray combustion instability for (i) $t_1 = 135.82$ ms, (ii) $t_2 = 136.19$ ms, (iii) $t_3 = 136.52$ ms, and (iv) $t_4 = 136.84$ ms.

by a t -test regardless of with or without downsampling. Note that, as shown in Fig. 1(c), the global dynamic behavior of an acoustic pressure field represents a limit cycle with large modulations in oscillation amplitudes.

Figure 3 shows the spatial distributions of the node strength s and vorticity ω , together with short-time variation in spatially averaged pressure $\langle p \rangle$. At t_1 corresponding to the local maximum of $\langle p \rangle$, an acoustic power source with high s is formed in the upstream region of the combustor ($0.5 \leq x/H \leq 2.0$), whereas at t_3 corresponding to the local minimum of $\langle p \rangle$, s takes high values near the upper wall of the combustor ($0.5 \leq x/H \leq 4.0$ and $1.0 \leq y/H \leq 1.3$). We do not observe acoustic power sources at t_2 and t_4 . The formation and collapse of acoustic power sources occur during spray combustion instability. As shown in Fig. 3(c), a large-scale organized vortex in response to a dominant acoustic mode is formed and detached at the step edge at t_1 . It collapses at t_3 . These results indicate that the formation and collapse of an acoustic power source are closely associated with the

motion of a large-scale organized vortex at the step edge. The time variation in average node strength $\langle s_i \rangle_y$ in terms of the y direction is shown in Fig. 4. We observe the aperiodic changes in the region where $\langle s_i \rangle_y$ takes high values over time. The acoustic pressure fluctuations take extreme values at $t = 112$ and 136 ms when $\langle s_i \rangle_y$ takes a high value. The node strength in the acoustic-energy-flux-based spatial network adequately extracts the formation region of the strong acoustic power source that drives spray combustion instability. The irregular formation of hubs in the network generated by a large-scale organized vortical structure plays an important role in the emergence of low-dimensional chaotic oscillations in the heat release rate field during spray combustion instability.

Figure 5 shows the spatial distribution of the symbolic dynamics-based synchronization index S_{SI} and the synchronization parameter $r_{p'q'}$. Both S_{SI} and $r_{p'q'}$ take high values in the upstream region of the combustor ($0.6 \leq x/H \leq 2.4$ and $0.4 \leq y/H \leq 0.7$). This indicates that spray combustion instability is driven in the upstream region, showing a strong

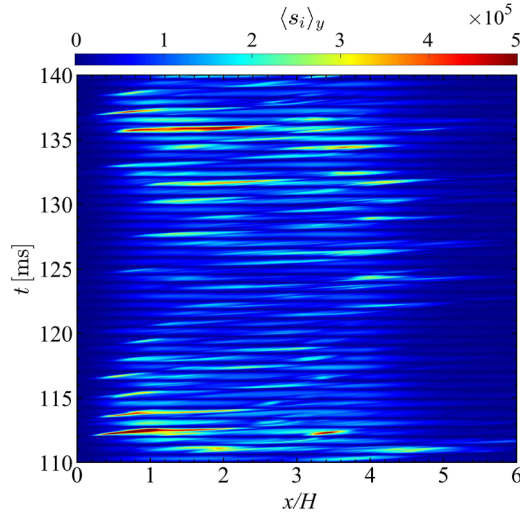


FIG. 4. Time variation in average node strength $\langle s_i \rangle_y$ in terms of the y direction in the acoustic-energy-flux-based spatial network.

phase-synchronized state between p' and q' . The formation region of high S_{SI} almost corresponds to that of the hub in an acoustic-energy-flux-based spatial network [Fig. 3(b)]. Asami *et al.* [25] and Mori *et al.* [42] have reported that the SDSI takes high values in the formation region of the detached large-scale vortex from a injector rim in a swirl-stabilized turbulent combustor. On the basis of the findings obtained by these studies [25,42], S_{SI} is found to be a useful measure for deducing the driving region of spray combustion instability in a backward-facing step combustor.

Figure 6 shows the spatial distribution of the feature importance $f_{m \rightarrow q}$ ($f_{\omega \rightarrow \Phi}$) for predicting heat release rate fluctuations (acoustic energy) from evaporation rate (vorticity) fluctuations. We observe locally high $f_{m \rightarrow q}$ at $x/H \approx 1.2$ and $y/H \approx 0.6$, indicating that the evaporation rate relatively predominates the heat release rate. A similar trend is observed for $f_{\omega \rightarrow \Phi}$ in the same region of x/H and y/H , which indicates that vorticity relatively predominates acoustic energy. The feature importance in a random forest is valid for

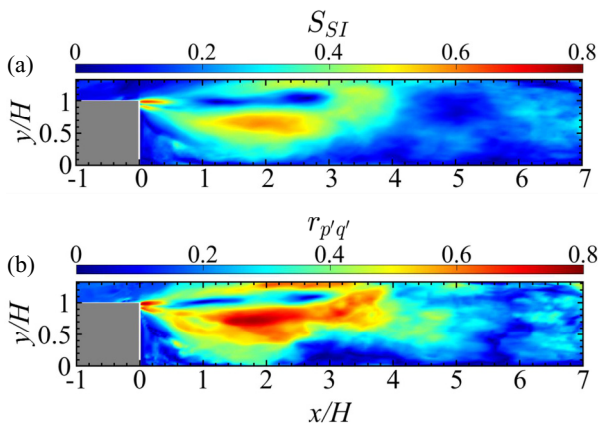


FIG. 5. Spatial distribution of the (a) symbolic dynamics-based synchronization index S_{SI} and (b) synchronization parameter $r_{p'q'}$ during spray combustion instability.

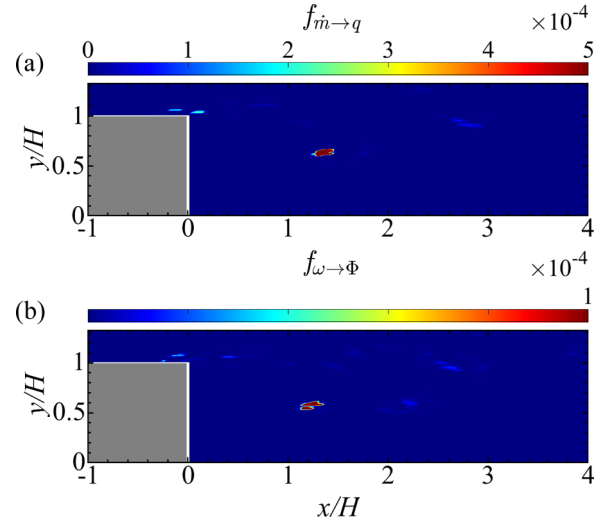


FIG. 6. Spatial distribution of the feature importance (a) $f_{m \rightarrow q}$ for the prediction of the heat release rate from evaporation rate fluctuations and (b) $f_{\omega \rightarrow \Phi}$ for the prediction of acoustic energy from vorticity fluctuations.

clarifying the feedback coupling of spray combustion instability. Pillai *et al.* [9] have reported that the entrainment of fuel droplets within a large-scale organized vortex increases their residence time, thereby increasing the evaporation rate. The ignition of premixture owing to the increase in evaporation rate induces the subsequent heat release. The high values of $f_{m \rightarrow q}$ at $x/H \approx 1.2$ and $y/H \approx 0.6$ fully support the findings obtained by Pillai *et al.* [9]. On the basis of the results shown in Figs. 3–6 and the findings reported by Pillai *et al.* [9], we are able to explain the formation mechanism of spray combustion instability in a backward-facing step combustor as follows. The hydrodynamic shear layer instability causes the formation and detachment of a large-scale organized vortex near the step edge. The entrainment by the organized vortex increases the residence time of the fuel droplets in the upstream region of the combustor and increases the evaporation rate. The fuel ignition in the upstream region induces a rapid increase in heat release rate, which results in a strong phase synchronization between acoustic pressure and heat release rate fluctuations. This strong phase synchronization leads to the formation of acoustic power sources. These physical processes play an important role in the driving and sustainment of spray combustion instability.

Mori *et al.* [42] have recently shown that reservoir computing [64], which is a class of supervised machine learning, is a useful recurrent neural network for clarifying the directional coupling of acoustic pressure and heat release rate fluctuations during combustion instability in a swirl-stabilized turbulent combustor. However, this method requires the optimization of many setting parameters during the learning process such as the size of the adjacency matrix in the reservoir network, leaking rate, and a regularization coefficient. In contrast, the main advantage of the feature importance in a random forest is that the number of setting parameters is small. This is very important when one wants to promptly know the causal connection between physical quantities during spray combustion

instability. Recent experimental studies [32,41,65] have adopted various causality analyses such as the transitivity [66] of joint recurrence and cross recurrence networks [67], cross convergent mapping [68], transfer entropy [69], symbolic transfer entropy [70], and spatial-network-based transfer entropy [41], for combustion instability in a swirl-stabilized and/or a bluff-body-stabilized turbulent combustor. In addition to these analytical methods, the importance in a random forest will become a useful machine-learning-based causality measure for understanding the feedback coupling during combustion instability.

Finally, there is an interesting concern related to the numerical simulation of spray combustion instability. Xu and co-workers [71–73] recently showed the importance of a discrete Boltzmann model to study both hydrodynamic and thermodynamic nonequilibrium effects in various fluid systems, including combustion systems [74,75]. It would be interesting to examine how this model is useful for simulating spray combustion.

IV. SUMMARY

We have numerically studied the dynamic behavior and driving region of spray combustion instability in a backward-facing step combustor using analytical methodologies based on dynamical systems theory, symbolic dynamics, complex networks, and machine learning. The global dynamic behavior of an acoustic pressure field represents a limit cycle with large modulation in oscillation amplitude. In contrast, the global dynamic behavior of a heat release rate field represents low-dimensional chaotic oscillations with deterministically aperiodic intercycle dynamics. This is clearly identified by the OPTN entropy in combination with IAAFT and PP surrogate data methods. The node strength in the acoustic-energy-flux-

based spatial network clearly shows that the formation and collapse of an acoustic power source during spray combustion instability are closely associated with the motion of a large-scale organized vortical structure owing to the hydrodynamic shear layer instability at the step edge. The irregular formation of hubs in the acoustic-energy-flux-based spatial network plays an important role in the emergence of low-dimensional chaotic oscillations in the heat release rate field. The driving region of spray combustion instability extracted using the SDSI is the formation and separation region of the organized vortex, which fairly corresponds to that of the hub in the acoustic-energy-flux-based spatial network. The order parameter identifies the formation of a strong phase synchronization between acoustic pressure and heat release rate fluctuations in the driving region of spray combustion instability. The feature importance in the random forest shows not only that the evaporation rate affects the heat release rate, but also that the vorticity affects the thermoacoustic energy. This feature importance enables us to clarify the feedback coupling of spray combustion instability.

ACKNOWLEDGMENTS

This work was partially supported by JSPS (Japan Society for the Promotion of Science) KAKENHI (Grants No. 22H00192 and No. 23K22691) and by MEXT (Ministry of Education, Culture, Sports, Science and Technology) via the Program for Promoting Researches on the Supercomputer Fugaku (Development of the Smart design system on the supercomputer Fugaku in the era of Society 5.0) (Grant No. JPMXP1020210316). This research used the computational resources of supercomputer Fugaku provided by the RIKEN Center for Computational Science (Project No. hp230193).

-
- [1] T. C. Liewen and V. Yang, *Combustion Instabilities in Gas Turbine Engines: Operational Experience, Fundamental Mechanisms, and Modeling* (AIAA, Reston, 2005).
 - [2] J. Keller, L. Vaneveld, D. Korschelt, G. Hubbard, A. Ghoniem, J. Daily, and A. Oppenheim, *AIAA J.* **20**, 254 (1982).
 - [3] D. A. Smith and E. E. Zukoski, *Proceedings of the AIAA/SAE/ASME/ASEE 21st Joint Propulsion Conference, Monterey, 1985* (AIAA, Reston, 1985).
 - [4] T. J. Poinso, A. C. Trouve, D. P. Veynante, S. M. Candel, and E. J. Esposito, *J. Fluid Mech.* **177**, 265 (1987).
 - [5] D. Thibaut and S. Candel, *Combust. Flame* **113**, 53 (1998).
 - [6] K. C. Schadow and E. Gutmark, *Prog. Energy Combust. Sci.* **18**, 117 (1992).
 - [7] R. Sampath, M. Mathur, and S. R. Chakravarthy, *Phys. Rev. E* **94**, 062209 (2016).
 - [8] T. Kitano, K. Kaneko, R. Kurose, and S. Komori, *Combust. Flame* **170**, 63 (2016).
 - [9] A. L. Pillai, J. Nagao, R. Awane, and R. Kurose, *Combust. Flame* **220**, 337 (2020).
 - [10] J. Nagao, A. L. Pillai, and R. Kurose, *J. Therm. Sci. Technol.* **15**, JTST0036 (2020).
 - [11] H. Gotoda, H. Nikimoto, T. Miyano, and S. Tachibana, *Chaos* **21**, 013124 (2011).
 - [12] H. Gotoda, M. Amano, T. Miyano, T. Ikawa, K. Maki, and S. Tachibana, *Chaos* **22**, 043128 (2012).
 - [13] H. Gotoda, Y. Shinoda, M. Kobayashi, Y. Okuno, and S. Tachibana, *Phys. Rev. E* **89**, 022910 (2014).
 - [14] V. Nair and R. I. Sujith, *J. Fluid Mech.* **747**, 635 (2014).
 - [15] V. Nair, G. Thampi, and R. I. Sujith, *J. Fluid Mech.* **756**, 470 (2014).
 - [16] M. Murugesan and R. I. Sujith, *J. Fluid Mech.* **772**, 225 (2015).
 - [17] H. Gotoda, Y. Okuno, K. Hayashi, and S. Tachibana, *Phys. Rev. E* **92**, 052906 (2015).
 - [18] Y. Okuno, M. Small, and H. Gotoda, *Chaos* **25**, 043107 (2015).
 - [19] L. Kabiraj, A. Saurabh, N. Karimi, A. Sailor, E. Mastorakos, A. P. Dowling, and C. O. Paschereit, *Chaos* **25**, 023101 (2015).
 - [20] H. Kobayashi, H. Gotoda, S. Tachibana, and S. Yoshida, *J. Appl. Phys.* **122**, 224904 (2017).
 - [21] S. Murayama, H. Kinugawa, I. T. Tokuda, and H. Gotoda, *Phys. Rev. E* **97**, 022223 (2018).
 - [22] S. Murayama and H. Gotoda, *Phys. Rev. E* **99**, 052222 (2019).
 - [23] Y. Guan, L. K. B. Li, B. Ahn, and K. T. Kim, *Chaos* **29**, 053124 (2019).
 - [24] Y. Fang, Y. Yang, K. Hu, G. Wang, J. Li, and Y. Zheng, *Phys. Fluids* **33**, 084104 (2021).

- [25] K. Asami, T. Kawada, S. Kishiya, and H. Gotoda, *Europhys. Lett.* **139**, 13001 (2022).
- [26] Z. Lyu, Y. Fang, Z. Zhu, X. Jia, X. Gao, and G. Wang, *Phys. Fluids* **34**, 054109 (2022).
- [27] K. Baba, S. Kishiya, H. Gotoda, T. Shoji, and S. Yoshida, *Chaos* **33**, 073101 (2023).
- [28] J. Ma, M. Han, X. Han, X. Hui, and X. Xue, *Phys. Fluids* **35**, 107125 (2023).
- [29] S. Mondal, V. R. Unni, and R. I. Sujith, *J. Fluid Mech.* **811**, 659 (2017).
- [30] S. A. Pawar, A. Seshadri, V. R. Unni, and R. I. Sujith, *J. Fluid Mech.* **827**, 664 (2017).
- [31] V. Godavarthi, V. R. Unni, E. A. Gopalakrishnan, and R. I. Sujith, *Chaos* **27**, 063113 (2017).
- [32] V. Godavarthi, S. A. Pawar, V. R. Unni, R. I. Sujith, N. Marwan, and J. Kurths, *Chaos* **28**, 113111 (2018).
- [33] A. Krishnan, R. I. Sujith, N. Marwan, and J. Kurths, *J. Fluid Mech.* **874**, 455 (2019).
- [34] R. I. Sujith and V. R. Unni, *Phys. Fluids* **32**, 061401 (2020).
- [35] R. I. Sujith and S. A. Pawar, *Thermoacoustic Instability: A Complex Systems Perspective* (Springer, Berlin, 2021).
- [36] R. Sampath and S. R. Chakravarthy, *Combust. Flame* **172**, 309 (2016).
- [37] T. Kobayashi, S. Murayama, T. Hachijo, and H. Gotoda, *Phys. Rev. Appl.* **11**, 064034 (2019).
- [38] T. Hachijo, S. Masuda, T. Kurosaka, and H. Gotoda, *Chaos* **29**, 103123 (2019).
- [39] G. Waxenegger-Wilfing, U. Sengupta, J. Martin, W. Armbruster, J. Hardi, M. Juniper, and M. Oswald, *Chaos* **31**, 063128 (2021).
- [40] Y. Shinchi, N. Takeda, H. Gotoda, T. Shoji, and S. Yoshida, *AIAA J.* **59**, 4086 (2021).
- [41] Y. Mori, S. Kishiya, T. Kurosaka, and H. Gotoda, *Phys. Rev. Appl.* **19**, 034097 (2023).
- [42] Y. Mori, T. Kawada, S. Fukuda, and H. Gotoda, *Proc. Combust. Inst.* **39**, 4671 (2023).
- [43] V. N. Vapnik, *IEEE Trans. Neural Networks* **10**, 988 (1999).
- [44] Y. LeCun, L. Bottou, Y. Bengio, and P. Haffner, *Proc. IEEE* **86**, 2278 (1998).
- [45] H. Jaeger, German National Research Center for Information Technology GMD Report No. 148, 2001 (unpublished).
- [46] T. Hashimoto, H. Shibuya, H. Gotoda, Y. Ohmichi, and S. Matsuyama, *Phys. Rev. E* **99**, 032208 (2019).
- [47] S. Shima, K. Nakamura, H. Gotoda, Y. Ohmichi, and S. Matsuyama, *Phys. Fluids* **33**, 064108 (2021).
- [48] K. Kawano, H. Gotoda, Y. Nabae, Y. Ohmichi, and S. Matsuyama, *J. Fluid Mech.* **959**, A1 (2023).
- [49] M. McCullough, M. Small, T. Stemler, and H. H.-C. Iu, *Chaos* **25**, 053101 (2015).
- [50] T. Schreiber and A. Schmitz, *Phys. Rev. Lett.* **77**, 635 (1996).
- [51] M. Small, D. Yu, and R. G. Harrison, *Phys. Rev. Lett.* **87**, 188101 (2001).
- [52] S. Leng, Z. Xu, and H. Ma, *Chaos* **29**, 093130 (2019).
- [53] J. Bellan and K. Harstad, *Int. J. Heat Mass Transf.* **30**, 125 (1987).
- [54] M. S. Miller, K. Harstad, and J. Bellan, *Int. J. Multiph. Flow* **24**, 1025 (1998).
- [55] M. S. Miller and J. Bellan, *J. Fluid Mech.* **384**, 293 (1999).
- [56] T.-W. Lee, J. E. Park, and R. Kurose, *At. Sprays* **28**, 241 (2018).
- [57] M. Small, in *Proceedings of the IEEE International Symposium on Circuits and Systems, Beijing, 2013* (IEEE, 2013), pp. 2509–2512.
- [58] C. Aoki, H. Gotoda, S. Yoshida, and S. Tachibana, *J. Appl. Phys.* **127**, 224903 (2020).
- [59] C. W. Kulp and L. Zunino, *Chaos* **24**, 033116 (2014).
- [60] T. C. Lieuwen, *Unsteady Combustor Physics* (Cambridge University Press, Cambridge, 2012).
- [61] L. Breiman, *Mach. Learn.* **45**, 5 (2001).
- [62] S. H. Strogatz, *Nonlinear Dynamics and Chaos*, 2nd ed. (CRC Press, Boca Raton, 2015).
- [63] V. Godavarthi, P. Kasthuri, S. Mondal, R. I. Sujith, N. Marwan, and J. Kurths, *Chaos* **30**, 033121 (2020).
- [64] J. Pathak, B. R. Hunt, M. Girvan, Z. Lu, and E. Ott, *Phys. Rev. Lett.* **120**, 024102 (2018).
- [65] T. Kurosaka, S. Masuda, and H. Gotoda, *Chaos* **31**, 073121 (2021).
- [66] M. E. Newman, *SIAM Rev.* **45**, 167 (2003).
- [67] N. Marwan, M. C. Romano, M. Thiel, and J. Kurths, *Phys. Rep.* **438**, 237 (2007).
- [68] G. Sugihara, R. May, H. Ye, C. Hsieh, E. Deyle, M. Fogarty, and S. Munch, *Science* **338**, 496 (2012).
- [69] T. Schreiber, *Phys. Rev. Lett.* **85**, 461 (2000).
- [70] M. Staniek and K. Lehnertz, *Phys. Rev. Lett.* **100**, 158101 (2008).
- [71] Y. Gan, A. Xu, H. Lai, W. Li, G. Sun, and S. Succi, *J. Fluid Mech.* **951**, A8 (2022).
- [72] D. Zhang, A. Xu, Y. Zhang, Y. Gan, and Y. Li, *Phys. Fluids* **34**, 086104 (2022).
- [73] D. Zhang, A. Xu, Y. Gan, Y. Zhang, J. Song, and Y. Li, *Phys. Fluids* **35**, 106113 (2023).
- [74] A. Xu, C. Lin, G. Zhang, and Y. Li, *Phys. Rev. E* **91**, 043306 (2015).
- [75] C. Lin, A. Xu, G. Zhang, and Y. Li, *Combust. Flame* **164**, 137 (2016).